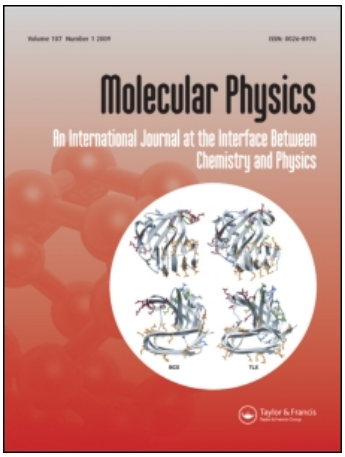

Molecular Physics
Publication details, including instructions for authors and subscription information:
http://www.informaworld.com/smpp/title~content=t713395160

A molecular dynamics simulation of interaction-induced FIR absorption spectra of liquid CS_2

Jannis Samios [a]; Uwe Mittag [a]; Thomas Dorfmüller [a]
[a] Fackultät für Chemie, University of Bielefeld, Bielefeld, F.R. Germany

Online Publication Date: 01 September 1986

To cite this Article Samios, Jannis, Mittag, Uwe and Dorfmüller, Thomas(1986)'A molecular dynamics simulation of interaction-induced FIR absorption spectra of liquid CS_2',Molecular Physics,59:1,65 — 79
To link to this Article: DOI: 10.1080/00268978600101911
URL: http://dx.doi.org/10.1080/00268978600101911

MOLECULAR PHYSICS, 1986, VOL. 59, NO. 1, 65–79

A molecular dynamics simulation of interaction-induced FIR absorption spectra of liquid CS_2

by JANNIS SAMIOS, UWE MITTAG
and THOMAS DORFMÜLLER†
Fackultät für Chemie, University of Bielefeld, 4800 Bielefeld, F.R. Germany

(Received 23rd December 1985; accepted 21st April 1986)

A molecular dynamics simulation of liquid CS_2 was carried out using site–site Lennard-Jones potentials. The total interaction-induced dipole correlation function was calculated by analysing the intermolecular interactions in self and cross terms as well as in different many-body correlation functions. The calculated correlation functions display large static and dynamic cancellation effects showing that a careful study of the various individual correlation functions is a necessary prerequisite for the understanding of the molecular dynamics of liquids. The present data display not perfect, but improved agreement with experimental far infrared absorption spectra as compared to previous simulations.

1. INTRODUCTION

At liquid densities the shape of interaction-induced spectra reflect CFs involving two, three, four and more particles. Any 'additivity' rule by which this many-particle character is bypassed is due to breakdown at sufficiently high densities depending upon the lowest order non-zero multipole of the dominant interaction and the geometrical anisotropy of the molecules.

The symmetry-forbidden interaction-induced spectra of pure liquid CS_2 and mixtures have been extensively studied experimentally by a number of authors [1–8]. Additionally the structure of liquid carbon disulphide and its dynamics have been studied by molecular dynamics (MD) computer simulation [9–11]. Since the present study has many common features to the paper of Madden and Tildelsley [11] to which we will refer often we use the shorthand notation MT. In MT the total induced dipole correlation function (CF) is expressed as a sum from contributions due to the polarization by the quadrupole tensor of the isotropic and the anisotropic part of the polarizability tensor and a cross term of these. This procedure is useful in allowing the study of the effect of the polarizability anisotropy, the answer to the question of the relative importance of the various n-body contributions remains, however, still incomplete. The simulation of the FIR absorption spectra in MT at 294, 244 and 291 K with densities along the SVP curve, has reproduced spectra with some discrepancies in shape and position of the maximum absorptivity as compared to the experimental spectra. Thus, at room temperature the peak height of the calculated spectrum is lower than the experimental by a factor of 1·5 and the position of the absorption maximum is located at $52\,cm^{-1}$ which means that it is displaced to lower frequencies by 15 wavenumbers.

Steele calculates the same CFs in a MD simulation of liquid nitrogen leaving the polarizability tensor $\alpha(t)$ unanalysed, but splitting the two sums into their separate n-body terms with $n = 2, 3, 4$ [12]. In the present analysis, which has been previously applied to CS_2 and N_2 [13, 14] the polarizability anisotropy has been taken into account by separately calculating the components parallel and normal to the symmetry axis of the linear molecule and from these calculating the respective CFs. On the other hand, by expressing the total moment CF as a sum of a self term C_s and a cross term C_+ between different molecules we include in the former n-body contributions with $n = 2, 3$ and in the latter n-body contributions with $n = 2, 3, 4$.

In the present study we have extended our analysis in the direction of Steele's approach by separating the various n-body contributions both of C_s and C_+ while keeping the analysis in terms of the parallel and the normal components of the induced dipole moment. As a result, we obtain a number of different CFs reflecting some of the details of the molecular dynamics of liquid CS_2. We have also carried out the calculations with an isotropic and an anisotropic polarizability model in order to obtain an insight into the effect of the reorientation of the reference molecule. We, furthermore, have carried out a comparison of the FIR spectra obtained from the present and previous simulations with available experimental data.

2. Theoretical

The spectroscopically observable total induced dipole moment $\mathbf{M}(t)$ of a system of molecules can be written as the sum of the induced dipoles of pairs, triplets, etc.

$$\mathbf{M}(t) = \sum \boldsymbol{\mu}_{ij} + \sum \boldsymbol{\mu}_{ijk} + \ldots . \tag{1}$$

In equation (1) $\boldsymbol{\mu}_{ij}(t)$ represents the moment induced on a reference molecule i by the molecule j through a given induction mechanism. In a first approximation, it has been often assumed that the three-body induced dipoles $\boldsymbol{\mu}_{ijk}(t)$ and higher order terms have little effect on the absorption spectrum. The equation 1 can be reduced to the first term, in which the sum involves only dipoles induced by pair-interactions for all pairs ij of molecules.

The total induced dipole CF, $C_M(t)$, which is a convenient representation of the time dependence reflected in the bandshape of the far-infrared (FIR) spectrum, is defined by the following equation:

$$\begin{aligned} C_M(t) &= \tfrac{1}{2}\langle \mathbf{M}(0) \cdot \mathbf{M}(t) + \mathbf{M}(t) \cdot \mathbf{M}(0) \rangle \\ &= \langle \mathbf{M}(0) \cdot \mathbf{M}(t) \rangle . \end{aligned} \tag{2}$$

The total absorption coefficient $\alpha(\omega)$ at angular frequency ω, which is a measure of the absorption of radiation due to the time dependence of the reorientation of the resultant induced dipole in the sample as reflected by the total dipole CF defined in equation (2), is linked to the Fourier transform of this CF by equation (3)

$$\alpha(\omega) = \frac{2(n^2 + 2)^2 \omega \tanh(\hbar\omega / k_B T)}{27 n \epsilon_0 V c \hbar} \int_0^\infty C_M(t) \cos \omega t \, dt. \tag{3}$$

n is the refractive index of the liquid assumed frequency independent. For absorption in the FIR region, n is generally equal to the value at high frequency. V is the volume of the system, c the speed of light and ϵ_0 the vacuum dielectric permittivity $((n^2 + 2)/3)^2/n$ is the Polo–Wilson local field correction factor and $\hbar^{-1} \tanh (\hbar\omega/2k_B T)$ an empirical quantum mechanical correction.

The interaction-induced absorption may be calculated theoretically from the dipoles induced by pairwise interactions which can be determined as a function of the relative molecular separations and orientations. To calculate the induced dipoles, one could, in principle, attempt to solve the quantum mechanical equations for the set of positions of pairs of molecules. Such a full quantum mechanical calculation is practically not feasible, with the possible exception of a few simple cases [15]. Consequently, the solution to this problem has been approximated by using an asymptotic multipole expansion model and in some cases corrections for the induction at short distances have been introduced [16, 17].

In this situation, molecular dynamics simulations have proved an invaluable tool in performing 'experiments' under controlled conditions with model molecules. We can thus calculate CFs which are experimentally accessible in real liquids and other CFs which, although not directly observable, may prove useful in allowing insight into some of the details of molecular dynamics of liquids. In nonpolar molecules the dipole moments induced in each molecule have mainly been interpreted on the basis of the following two of assumptions. Firstly, it is assumed that the local electric field $\mathbf{F}_{ij}$ at the centre of the molecule i obtained by means of a point multipole expansion adequately describes the effect of the inducing molecule j. Secondly, the point polarizability assumption is made, which states that the polarizable matter of the molecule can be considered to act as if it were concentrated at the molecule's centre of mass. Both assumptions are not without risk if the intermolecular separation is small as it is the case at liquid densities. In a more complete calculation one would calculate electric field first gradients $\nabla\mathbf{F}_{ij}$, second gradients $\nabla\nabla\mathbf{F}_{ij}$ and so forth, which may contribute to the induced dipole moment. Then, we could calculate the induced moment $\boldsymbol{\mu}_{ij}$ by means of equation (4).

$$\boldsymbol{\mu}_{ij} = \boldsymbol{\alpha}_i \mathbf{F}_{ij} + \tfrac{1}{3}\boldsymbol{A}_i : \nabla\mathbf{F}_{ij} + \tfrac{1}{15}\boldsymbol{E}_i : \nabla\nabla\mathbf{F}_{ij} + \ldots . \tag{4}$$

The electric field gradient and the second gradient correspond to the $\boldsymbol{A}$ and $\boldsymbol{E}$ polarizability, being third and fourth rank tensors respectively. In the particular case of $D_{\infty h}$ symmetry of linear molecules (see table 1) the $\boldsymbol{A}$ tensor does not exist and the contribution from the field-gradient term in equation (4) is zero. On the other hand, the tensor $\boldsymbol{E}$ exists and therefore second gradients may contribute to the induced dipole. However, we assume that this contribution is not important and we thus neglect this effect.

Table 1

Tensor molecular Symmetry	Independent components						
	μ^0_α	$Q^0_{\alpha\beta}$	$\Omega^0_{\alpha\beta\gamma}$	$\phi^0_{\alpha\beta\gamma\delta}$	$\alpha_{\alpha\beta}$	$A_{\alpha\beta\gamma}$	E_{ab}
$D_{\infty h}$	0	1	0	1	2	0	2

Assuming that both the quadrupole and the hexadecapole, contribute to the electric field at the distances involved equation (5) describes the induced field on molecule i due to the molecule j

$$F_{ij}^{\alpha}(t) = F_{ij}^{\alpha,Q}(t) + F_{ij}^{\alpha,\phi}(t). \tag{5}$$

Q and ϕ are the molecular quadrupole and hexadecapole moments. The configurational space of the system is defined by the vector $\mathbf{R}_{ij}$ between the molecule i and j and by the unit vector $\hat{u}_i = \hat{u}_i(u_i^{\alpha}, u_i^{\beta}, u_i^{\gamma})$ along the molecular axis of the molecule i with respect to the laboratory reference system. The induced field $\mathbf{F}_{ij}$ is analysed into a component parallel to the molecular axis $\mathbf{F}_i^{\parallel}$ and a component normal to it $\mathbf{F}_i^{\perp}$ as follows:

$$\mathbf{F}_{ij}^{\parallel} = [\mathbf{F}_{ij} \cdot \hat{u}_i]\hat{u}_i, \tag{6a}$$

$$\mathbf{F}_{ij}^{\perp} = \mathbf{F}_{ij} - \mathbf{F}_{ij}^{\parallel}. \tag{6b}$$

Finally, equations (7 *a*) and (7 *b*) describe the induced dipole moment $\boldsymbol{\mu}_{ij}$ on the molecule i, on the basis of an isotropic and an anisotropic molecular polarizability model respectively

$$\boldsymbol{\mu}_{ij}(t) = \alpha \mathbf{F}_{ij}(t), \tag{7a}$$

$$\boldsymbol{\mu}_{ij}(t) = \alpha^{\perp}\left[\left(\frac{\alpha^{\parallel}}{\alpha^{\perp}}\right)\mathbf{F}_{ij}^{\parallel}(t) + \mathbf{F}_{ij}^{\perp}(t)\right]. \tag{7b}$$

The total dipole CF $C_{\mathrm{M}}(t)$ from equation (2) can be written as

$$C_{\mathrm{M}}(t) = \sum_{ij}\sum_{kl} \langle \boldsymbol{\mu}_{ij}(0) \cdot \boldsymbol{\mu}_{kl}(t) \rangle. \tag{8}$$

The total induced dipole moment on each molecule is

$$\boldsymbol{\mu}_i(t) = \sum_{j \neq i} \boldsymbol{\mu}_{ij}(t). \tag{9}$$

We first split the sum in equation (8) into a self- and cross-CF: $C_{\mathrm{s}}(t)$ and $C_{+}(t)$ defined as follows:

$$C_{\mathrm{M}}(t) = C_{\mathrm{s}}(t) + C_{+}(t), \tag{10a}$$

$$C_{\mathrm{s}}(t) = \sum_{i} \langle \boldsymbol{\mu}_i(0) \cdot \boldsymbol{\mu}_i(t) \rangle, \tag{10b}$$

$$C_{+}(t) = \sum_{\substack{i,j \\ i \neq j}} \langle \boldsymbol{\mu}_i(0) \cdot \boldsymbol{\mu}_j(t) + \boldsymbol{\mu}_j(0) \cdot \boldsymbol{\mu}_i(t) \rangle. \tag{10c}$$

The self term describes the time evolution of the dipole moment induced on a given reference molecule by the cage molecules. The cross-term describes the time evolution of the magnitude and the relative position of two induced dipole moments averaged over all molecule pairs ij in the sample. By splitting the sum of equation (10 *b*) into the n-body CFs with $n = 2, 3, 4$ we obtain only two distinct CFs defined by equations (11 *a*) and (11 *b*)

$$C_{2A}(t) = \sum_{i \neq j} \langle \boldsymbol{\mu}_{ij}(0) \cdot \boldsymbol{\mu}_{ij}(t) \rangle, \tag{11a}$$

$$C_{3A}(t) = \sum_{\neq} \langle \boldsymbol{\mu}_{ij}(0) \cdot \boldsymbol{\mu}_{ik}(t) \rangle. \tag{11b}$$

The analysis of the sum of equation (10 *c*) gives the following CFs defined by equations (12 *a–e*)

$$C_{2B}(t) = \sum_{i \neq j} \langle \boldsymbol{\mu}_{ij}(0) \cdot \boldsymbol{\mu}_{ji}(t) \rangle, \tag{12a}$$

$$C_{3B}(t) = \sum_{\neq} \langle \boldsymbol{\mu}_{ij}(0) \cdot \boldsymbol{\mu}_{ki}(t) \rangle, \tag{12b}$$

$$C_{3C}(t) = \sum_{\neq} \langle \boldsymbol{\mu}_{ij}(0) \cdot \boldsymbol{\mu}_{kj}(t) \rangle, \tag{12c}$$

$$C_{4C}(t) = \sum_{\#} \langle \boldsymbol{\mu}_{ij}(0) \cdot \boldsymbol{\mu}_{kl}(t) \rangle. \tag{12d}$$

In these equations $\neq$ denotes that the summation extends over all values of i, j, k which are different to each other and $\#$ denotes that the summation extends over all i, j, k, l which are different to each other. The CFs are indexed according to the character of the interaction. Thus, the first index indicates the number of molecules involved. CFs in which the dipole moment of molecule i at time 0 is correlated to the dipole moment of the same molecule i at time t are indexed with the letter A as a second index. The indices B and C designate CFs where the dipole of molecule i at time 0 is correlated with the dipole of another molecule j or k at time t the difference between B and C being that in the former case the two molecules whose dipole moments are correlated interact directly whereas they interact via another molecule when the second index is C. This notation somewhat differs from the one introduced for the first time by Steele [12]. Figure 1 is a pictorial representation of the interactions responsible for the CFs defined in equations (11 *a, b*) and (12 *a–d*).

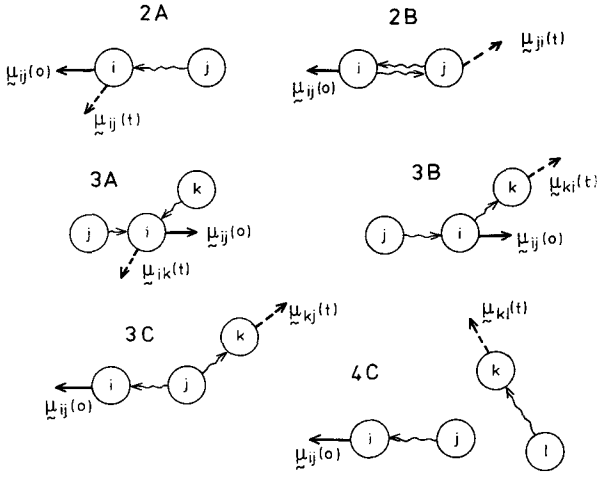

Figure 1. Pictorial representation of the two-, three- and four-n-body interaction-induced dipole CFs defined in equations (11 *a, b*) and (12 *a–d*). The solid arrows represent the induced dipole at time 0, the broken arrows a dipole at a later time t and the wavy arrows the interaction considered in this particular interaction model. To each dipole arrow corresponds an interaction arrow as indicated.

3. The molecular dynamics simulation

The molecular dynamics simulation was carried out on the basis of a Lennard-Jones atom–atom potential. The molecules were taken to be rigid linear triatomics. Throughout the simulation periodic boundary conditions have been used to simulate the infinite system. The potential parameters used in the simulation were identical to those used in a previous simulation of liquid CS_2 [10, 13]. The C–S bond length was 1·56 Å and the potential cutoff was set at half the box length $L/2$. The initial temperature was 298 K and the density $d = 1{\cdot}26\,\mathrm{g\,cm^{-3}}$. The initial configuration used in the simulation was a f.c.c. lattice. In this starting configuration the orientation of each molecule has been selected randomly. The molecular velocities (translation and rotational) were assigned so that the net centre of mass velocity and the angular velocity of the system were both zero and the kinetic energy corresponds to the initial temperature. In order to check the consistency of the calculations two simulations with exactly the same input data were carried out independently from each other. In the first one, the equations of motion were integrated by the standard Verlet–Singer algorithm [18] over 52 ps with a time step $\Delta t = 10^{-15}$ s and over 256 molecules. In the second simulation a quartenion predictor corrector algorithm [19] was used with a time step of $\Delta t = 5{\cdot}10^{-15}$ s and 108 molecules. This simulation was extended to approximately 80 ps. For both simulations equilibrium was achieved after approximately 10 ps. The data were stored at time intervals of 0·025 ps. The equilibrium properties calculated from both simulations were in good agreement with the corresponding experimental data and with those reported in previous simulations [10]. During the simulation we have stored all molecular positions, orientations and velocities in intervals of 5 steps (0·025 ps time intervals) over a total time interval of 75 ps. The various CFs have been calculated by a subsequent analysis of the stored data on magnetic tapes. For each stored configuration the induced dipoles $\boldsymbol{\mu}_{ij}(t)$ have been obtained for all pairs $i \neq j$ with the condition $R_{ij} \leqslant R_c = L/2$. The total induced dipole moment $\mathbf{M}(t)$ of the box and of each molecule $\boldsymbol{\mu}_i(t)$, has also been obtained from the induced moments $\boldsymbol{\mu}_{ij}(t)$ by means of equations (1) and (9). The differences between the simulated values of the effective molcular dipole moments μ_{eff} for both simulations were negligible. This means that the contribution of molecules more distant than approximately 10 Å can be neglected. It was also checked in our previous simulation of liquid N_2 that the used cutoff radius of $L/2$ corresponding to 10 Å could reproduce extremely well the experimental effective dipole moment using a quadrupole induction mechanism.

In order to obtain adequate precision for the calculated CFs, we have extended these calculations over a large number of time origins and over all molecules of the sample. Due to the periodic boundary conditions at longer times an incertitude in the CFs may develop. In order to achieve a reliable time evolution in the range 0–1 ps, where all experimental CFs lie, the most important CFs have been obtained from MD runs extending over a total time interval of 70 ps for a large number of time-origins and over all molecules. Particularly, the accuracy of the shape of the total CF at time above 0·6 ps is not satisfactory if the statistics are sampled only at times below 35 ps with 108 molecules. We have also compared the calculated CFs from both simulations between 0–1 ps and no differences have been observed. The calculation of the n-body CFs has been carried out separately from the second simulation. These also have been calculated for a large number of time-origins and over all molecules. We have observed that if the

statistics were sampled over times above 40 ps the accuracy of the CFs were fairly stable between 0–1 ps. The above procedure led to an acceptable statistical error which was larger for the total, cross and four-body CFs than for the self two-, and three-body CFs.

In order to obtain the FIR spectrum corresponding to the simulated total dipole-CF the transformation of the latter was carried out by numerical Fourier transformation using equation (3) and, independently, using a three-variable Mori transform, which was used in previous work [14].

4. Results and discussion of the correlation functions

The analysis of the total dipole CF as obtained by equations (10 *a–c*) is illustrated in figure 2. We see that the directly measurable $C_M(t)$ has a relatively small amplitude in contrast to the self-CF $C_s(t)$. This can be formally traced back to the large negative value of the cross-CF $C_+(t)$ since the three CFs are connected by equation (10 *a*). In the stationary case, i.e. in the zero-timeshift limit, $C_M(0)$ is smaller by a factor of 5·5 as compared to the corresponding single-molecule CF $C_s(0)$. As time proceeds $C_s(t)$ and $C_+(t)$ approach each other in long-time tails with the consequence that $C_M(t)$ decays to zero at a faster rate than either $C_s(t)$ or $C_+(t)$. This result clearly illustrates the important dynamic cancellation due to the relative motion of different molecules both in the amplitude and the time evolution of the observable total dipole CF. A similar result has been observed for liquid N_2 [14]. Both results show that the neglect of intermolecular cross-correlations amounts to ignoring an essential part of the line-shaping mechanism in far-infrared absorption spectra of liquids.

The separation of the observed dipole CF into a cross and a self term is not meant to imply that single molecule motions and collective motions have been thus separated. The CF C_s which describes the time evolution of the dipole induced on a given molecule contains all of the many-body interactions resulting in a time-dependent induced dipole moment $\boldsymbol{\mu}_i(t)$. The separation of single molecule dynamics from the collective dynamics is still awaiting a satisfactory solution. The separate calculation of two-body, three-body and four-body CFs described below is only a step in this direction.

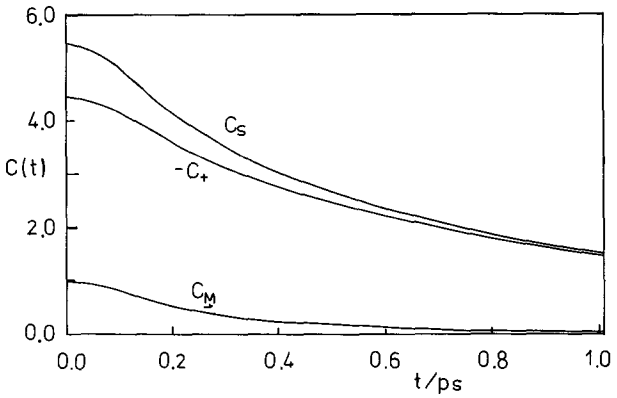

Figure 2. Comparison of the simulated total-CF, self-CF and cross-CFs of liquid CS_2 at 298 K with the anisotropic polarizability model.

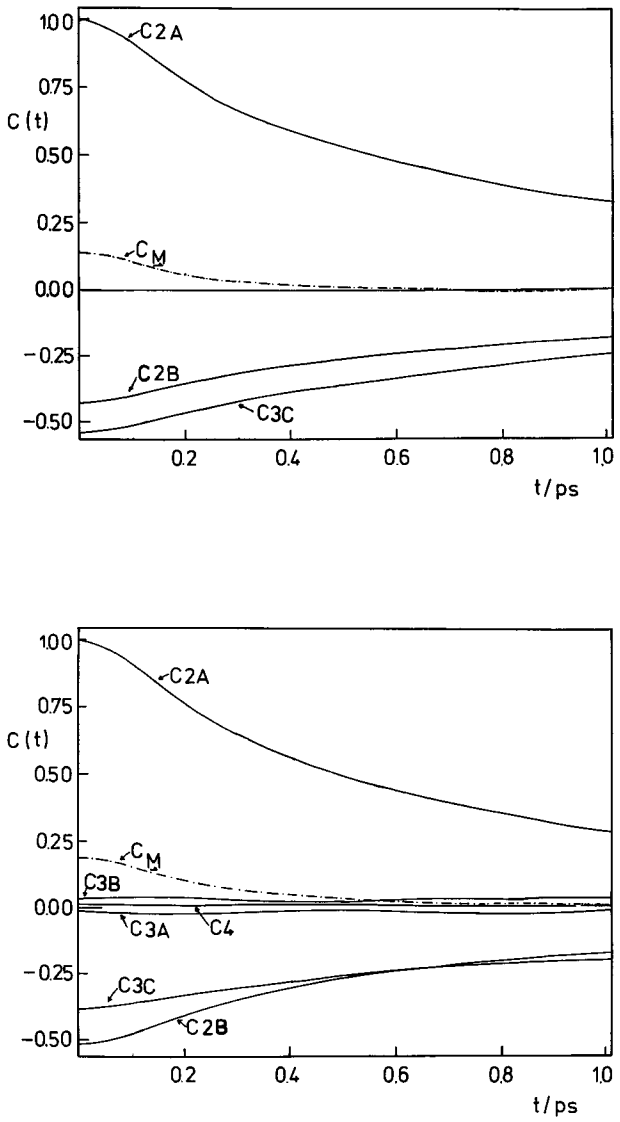

Figure 3. The individual many-body CFs as illustrated in figure 1 for the isotropic and anisotropic polarizability models.

Figure 3 (*a*) displays the simulated two-, three- and four-body CFs, for the isotropic and the anisotropic polarizability models respectively, where all CFs have been normalized with respect to $C_{2A}(0)$. One can see that for both models C_{2B}, C_{3C} and C_{3A} are negative. C_{4C} however, is negative for the isotropic and positive for the anisotropic model. Table 2 gives the values of CFs at $t = 0$, for both polarizability models used and for two experimental values of the quadrupole moment. The CFs have been also normalized with respect to $C_{2A}(0)$. By using the absolute magnitudes of $C_M(0)$ per molecule in relative units (see table 2) we can easily calculate the corresponding values of all these CFs.

Table 2. Quadrupole interaction induced dipole CFs at zero time for isotropic and anisotropic polarizability model [20]. Comparison of experimental and simulated values of the effective dipole moment $\mu_{eff}/10^{-31}$ C m per molecule.

Polarizability	$CF_s(0)/C_{2a}(0)$							$\mu_{eff}/30^{-31}$ C m		
Model								Calculated used quadrupole moment 10^{-40} C m^2		Experimental
	C_{2A}	C_{2B}	C_{3A}	C_{3C}	C_{3B}	C_{4C}	C_M	12·0 [21]	9·3 [22]	
Isotropic	1·000	−0·423	−0·004	−0·534	0·065	−0·029	0·139	4·59	3·56	3·46 [4(2)]
										3·6 [2]†
								5·44	4·22	
Aniso-tropic	1·000	−0·513	−0·006	−0·372	0·032	0·012	0·184			3·64 [6]
								5·74 [11]		

† Calculated from the fit parameters given by the authors.

Both $C_s(t)$ and $C_+(t)$ can be written in terms of the above n-body CFs as follows:

$$C_s(t) = C_{2A}(t) + C_{3A}(t), \tag{13a}$$

$$C_+(t) = C_{2B}(t) + C_{3C}(t) + 2C_{3B}(t) + C_{4C}(t). \tag{13b}$$

The negative sign of some of these CFs which seems to be a general feature can be rationalized as follows: In the case of $C_{2B}(t)$, neglecting for the moment orientational effects, the two induced dipole moments which are being correlated (see figure 1) result from opposite pair configurations in space and will be vectors tending to align in opposite directions. In the case of the $3A$- and the $3C$-type CFs a similar argument may hold. If a molecule k is in a given position near molecule j, as illustrated in figure 1 for example for the $3C$-type interaction, then the probability that a third molecule i be located on the opposite side with respect to a plane passing through the centre of j normal to the line joining the centres of k and j is larger than the probability that it is located on the same side. Thus, averaging the effect of the relative orientation of the molecules, the dipole vectors induced from j to k and i or the dipoles induced on j by k and i will point on the average in opposite directions and the scalar product of the two dipole vectors will be negative. The CF of the type $3B$ on the other side would be expected to be positive as illustrated in figure 1. These qualitative arguments which completely neglect the shapes of the multipole fields and the orientational correlations of adjacent molecules seem to justify the signs observed for the simulated CFs. The signs discussed above and observed in this simulation are identical to those observed by Steele for N_2 with the only exception of $3B$ (in his notation $3c$) which is positive for CS_2 and negative for N_2. However, different signs cannot be excluded and if they are observed they point to the occurrence of particular orientational correlations for a given liquid. Gibson and Dore have found by analysing their neutron scattering data [23] that a configuration in which the CS_2 molecules are arranged normally to two other forming an angle of 60° is a preferred one. We have calculated the signs of the $2B$ and $3C$-type CFs for this particular configuration and the signs are indeed the same as observed in this MD simulation.

Figure 3 also shows that the dominant CFs in liquid CS_2 are the $2A$, $2B$ and $3C$ the latter two being negative. The contribution of the other three calculated CFs, i.e. $3B$, $3A$ and $4C$ is extremely small (of the order of 1 per cent or less). The CFs $2B$, $3A$, $3C$, $3B$ and $4C$ contain single non-zero rank spherical tensors (quadrupole-tensor) on two or more different molecules. If one neglects the local orientational correlations in the liquid, then these CFs must vanish as they depend upon the second-order Legendre polynomial CF $P_2(\cos(\theta_{ij}(0)))$ where $\theta_{ij}(0)$ is the relative orientation of molecules i and j at $t = 0$. It appears that these CFs may be sensitive indicators of local orientational order in liquids. In a qualitative way, under the simplifying assumptions illustrated in figure 1, it can be shown that indeed C_{2A} is expected to have the largest amplitude of all CFs since for $t = 0$ it does not contain contributions from unfavourable configurations. Table 2 summarizes the various calculated n-body CFs in the static limit for the two models. Contrary to the situation in less anisotropic molecules, as nitrogen, the differences between the two models illustrated in figures $3a$ and $3b$ are non-negligible and reflect the effect of static and dynamic orientational correlations. Thus, the relative magnitude of C_{2B} and C_{3C} are inverted and the decay curves of C_{2B} are clearly different in the two models. The cancellation between C_{2A} on the one side and C_{2B} together with C_{3C} on the other reduces the observed CF to 10 per cent of C_{2A}. This shows the importance of a separate study of the various n-body CFs for the understanding of the details of the molecular dynamics of a liquid.

Figure 4 displays the calculated $C_{2A}(t)$ (curve 1 and 2) for the isotropic and the anisotropic polarizability models respectively and the second-order Legendre polynomial-CF $C_2(t) = P_2(\cos\theta(t))$ (curve 3). The curve indicated by 4 displays the time evolution of the ratio $C_{2A}(t)/C_2(t)$ which reflects the translational CF of the molecules. We can see that this translational CF decays more slowly than the rotational CF over the whole timerange. It thus appears that $C_{2A}(t)$ is dominated by molecular reorientation. The simulated $C_{2A}(t)$ of liquid nitrogen is included in the figure (curve 5) as a comparison showing the large difference between these molecules, the correlation times differing by a factor of 4. The comparison of some of the various n-body CFs for the two polarizability models is made in

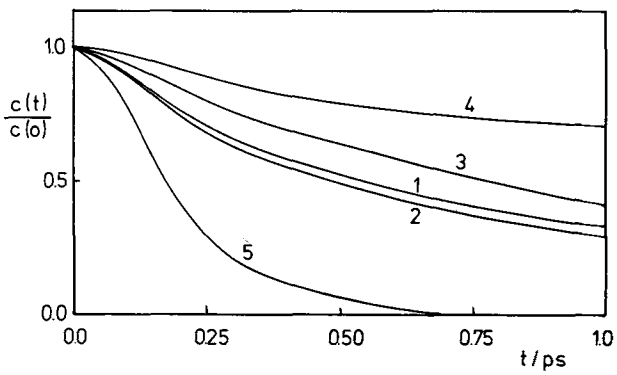

Figure 4. Comparison between various calculated CFs normalized to one. 1, $C_{2A}(t)$: isotropic polarizability model; 2, $C_{2A}(t)$: anisotropic polarizability model; 3, $P_2(\cos\theta(t))$: second order Legendre reorientation CF from this simulation; 4, $C_{TR}(t)$: translational CF; 5, $C_{2A}(t)$: from MD simulation of liquid N_2 at 74 K [12].

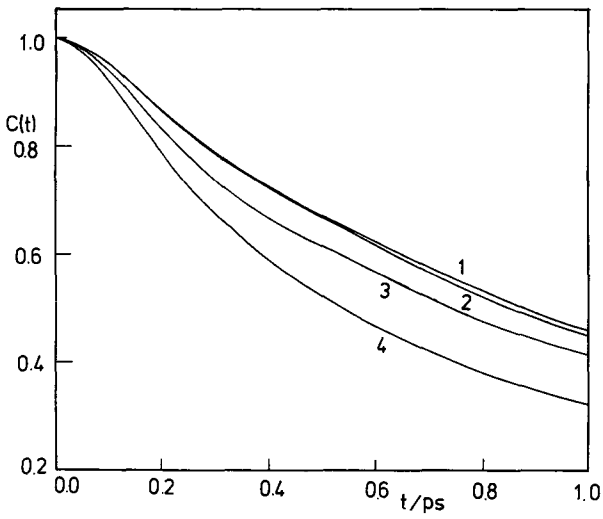

Figure 5. Comparison between various CFs normalized to one. 1, $C_{3C}(t)$: anisotropic polarizability model; 2, $C_{2B}(t)$: isotropic polarizability model; 3, $C_{3C}(t)$: isotropic polarizability model; 4, $C_{2B}(t)$: anisotropic polarizability model.

figure 5. We can see that the result depends quite significantly upon the used polarizability model, that whereas for the $2B$-type CF the anisotropic model predicts a faster decay the opposite is the case for the type 3C-CF. This result again indicates the usefulness of considering separately the various n-body CFs for analysing the details of the molecular dynamics.

5. Comparison with experimental far infrared spectra

In order to check the underlying model of the simulation, i.e. the multipole expansion with a quadrupole as the leading term for the CS_2–CS_2 interaction, we have compared the results with experimental data obtained by far infrared absorption of the interaction induced dipoles. Figure 6 displays the total dipole CF obtained by Fourier transforming the three-variable Mori fit of the experimental spectrum at 298 K and the simulated $C_M(t)$. The discrepancy is obvious and is, of course, also reflected in the comparison illustrated in figure 7 of the experimental spectra with the spectra obtained from the simulation normalized to a common amplitude. Since the amplitude of the spectra obtained from simulated CFs depends upon the value of the quadrupole moment used and since the values reported in the literature for Q are different we have represented in figure 8 two different simulated spectra corresponding to the extreme experimental values of Q. The shaded region defines the very large incertitude as to the true value of the amplitude. We see that the experimental spectrum obtained in our laboratory, indicated by the dashed line, lies within the range of the present simulated values. However, one can also see that our experimental spectrum is displaced to higher frequencies as compared to the simulated spectra. Figure 8 also displays the spectrum simulated in MT, represented by the squares, which lies significantly below both the spectra given by the present simulation and the experimental spectrum. More specifically, using the same parameters as

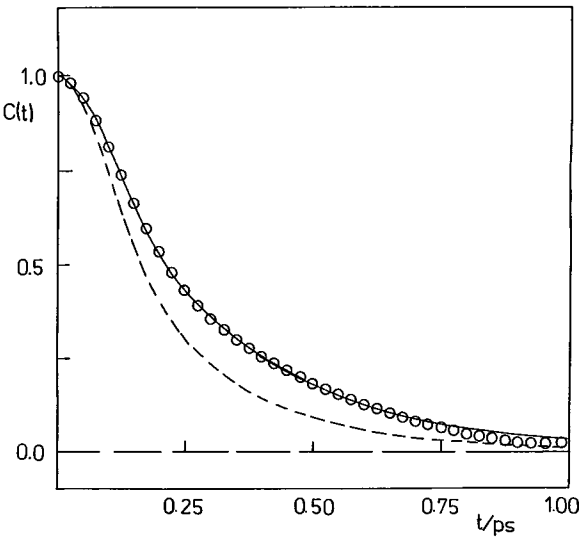

Figure 6. Total interaction induced dipole CFs. The dashed line represents the CF obtained from the Fourier transform (Mori fit) of the experimental FIR spectrum. The circles represent the simulated (anisotropic polarization model) total CF and the solid line is obtained by the fit of the Mori function to the above points.

in MT ($Q = 12{\cdot}0 \times 10^{-40}\,\mathrm{C\,m^2}$, $\alpha = 9{\cdot}3 \times 10^{-40}\,\mathrm{C^2\,m^2\,J^{-1}}$, $\Delta\alpha = 11{\cdot}18 \times 10^{-40}\,\mathrm{C^2\,m^2\,J^{-1}}$), we obtain a simulated spectrum whose peak height is more than the experimental value by a factor 1·6 whereas the spectrum of MT lies below the experimental by a factor of 1.4. No available experimental value of the quadrupole moment is able to shift the simulated spectrum in MT near the experimental spectrum. On the other hand, we were able to obtain FIR spectra from the simulated CFs which seem to be in somewhat better agreement with experimental spectra by using a different experimental value for the molecular quadrupole ($Q = 9{\cdot}3 \times 10^{-40}\,\mathrm{C\,m^2}$). This value of Q has been obtained by a semi-experimental method combining *ab initio* calculations. Given the large

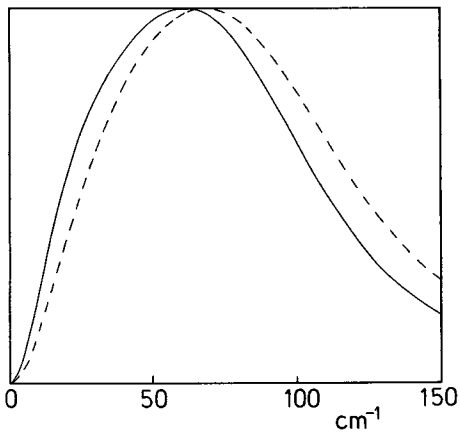

Figure 7. Experimental (dashed line) and simulated (solid line) spectrum (anisotropic polarization model), both normalized to the same amplitude.

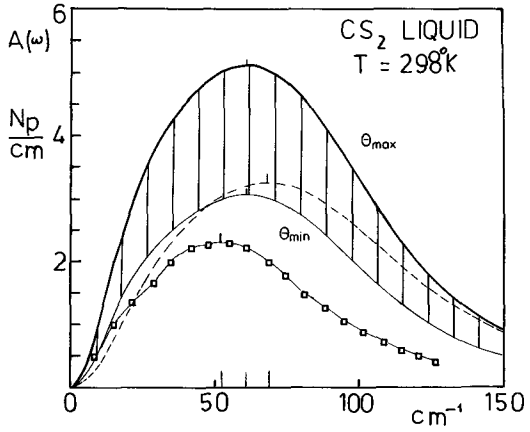

Figure 8. Direct comparison between experimental and simulated spectra of liquid CS_2 (anisotropic model). The dashed line represents the experimental spectrum. The shaded range illustrates the range in which the simulated spectrum lies, considering the uncertainty in the experimental value of the quadrupole moment. The simulated spectrum was obtained by the Mori fit. The squares represent the simulated spectrum in MT.

errors in the experimental determination of Q it is difficult to estimate whether the true value for CS_2 lies nearer to 12 or to 9·3. In any case while the experimental spectrum lies within the shaded area given by our simulation, while the MT simulated spectra would give the analogous shaded area below this, whatever value of Q between 12 and 9·3 is chosen, we consider the present result as an improved, albeit not perfect, agreement with experiment.

The position of the calculated absorption maximum in MT is located at $52\,cm^{-1}$ i.e. it is shifted by $15\,cm^{-1}$ to lower values relative to the experimental spectrum lying at $67\,cm^{-1}$, whereas the spectrum obtained by the present simulation is shifted with respect to the experimental spectrum by 7 wavenumbers only. In both cases the spectral lineshape displays differences as compared to the experiment.

The discrepancies between the simulated spectra are remarkable as both calculations were performed with the same algorithm and the same potential. The difference between the two procedures lies in the method used to calculate the spectra from the CFs. Thus, whereas MT use the maximum entropy method for this purpose, in the present calculations the three-variable Mori relation was used to fit the CFs and to perform the Fourier transform analytically by means of equations 10, 11, 12 of [14]. It might be the case that the Mori fit better represents the curvature of the short-time section of the CF than the maximal entropy method. However, the differences which might result from the use of such different procedures are presently difficult to assess. In conclusion, it appears that although both simulations do not reproduce the experimental spectra completely the present results are in better agreement with experiment both with respect to the amplitude and to the position of the absorption maximum. However, the discrepancies between the spectra obtained by the two simulations while the effective dipole moments as, illustrated in table 2, are identical within the computation error range indicate an inconsistency which should be resolved by a common effort.

6. Summary

The present simulation was undertaken in order to analyse in more detail than previous simulations the molecular dynamics of liquid CS_2. For this purpose extreme care was taken to ensure reliable statistics. The obtained CFs were analysed into self- and cross-CFs and furthermore into various many-body CFs. It was shown that the cancellation leading to the total dipole CF sensitivity depends upon the time evolution of the various CFs calculated and that these latter also depend upon the polarizability model used. It is shown that the present simulation compares more favourably to experimental spectra than previous simulations but also that the lineshapes still are in need of improvement, probably by introducing a more sophisticated model for the inducing mechanism. This could be achieved by introducing a hexadecapole and, if necessary, some form of an electron overlap interaction.

Because of the importance of the various CFs obtained from the simulation we are presently examining the possibility to reproduce analytically such many-body CFs. This model will be described in a forthcoming publication.

This work was performed within the project 'Complex Liquids' of the 'Zentrum für interdisziplinäre Forschung' of the University of Bielefeld whose support is gratefully acknowledged. We also acknowledge the financial support of the DFG, and the 'Fonds der Chemischen Industrie'.

References

[1] Garg, S. K., Bertie, J. E., Kilp, H., and Smyth, C. P., 1969, *Chem. Phys.*, **49**, 2551. Darmon, I., Gerschel, A., and Brot, C., 1971, *Chem. Phys. Lett.*, **8**, 454.

[2] Kettle, J. P., and Price, A. H., 1972, *J. chem. Soc. Faraday Trans. II*, **68**, 1306.

[3] Davies, G. J., Chamberlain, J., and Davies, M., 1973, *J. chem. Soc. Faraday Trans. II*, **69**, 1223. Davies, G. J., and Chamberlain, J., 1973, *J. chem. Soc. Faraday Trans. II*, **69**, 1739.

[4] Evans, M., and Davies, G. J., 1976, *J. chem. Soc. Faraday Trans. II*, **72**, 1206. Davies, G. J., and Evans, M., *J. chem. Soc. Faraday Trans. II*, **72**, 1194. Davies, G. J., and Evans, M., 1976, *Chem. Phys. Lett.*, **41**, 521.

[5] Fujiwara, K., Ikowa, S., and Kimara, M., 1979, *Bull. chem. Soc. Japan*, **52**, 227.

[6] Potthast, L., Samios, J., and Dorfmüller, Th., 1986, *Chem. Phys.*, **102**, 147.

[7] Evans, J. C., and Bernstein, H. J., 1956, *Can. J. Phys.*, **34**, 1127. Tabisz, G. C., 1978, *Molecular Spectroscopy*, Vol. 6, edited by R. F. Barrow and D. A. Long (Chemical Society). Perchard, J. P., 1978, *Proc. 6th Int. Conf. on Raman Spectroscopy*, Vol. I, p. 235.

[8] Cox, T. I., and Madden, P. A., 1976, *Chem. Phys. Lett.*, **41**, 195; see also 1980, *Molec. Phys.*, **39**, 1487; 1981, *Molec. Phys.*, **43**, 307. Madden, P. A., and Cox, T. I., 1981, *Molec. Phys.*, **43**, 287. Weiss, E., and Dinur, V., 1983, *Chem. Phys. Lett.*, **99**, 197.

[9] Steinhauser, O., and Neumann, M., 1979, *Molec. Phys.*, **37**, 1921. Steinhauser, O., 1981, *Chem. Phys. Lett.*, **83**, 153.

[10]. Tildesley, D. J., and Madden, P. A., 1981, *Molec. Phys.*, **42**, 1137; see also 1982, *Molec. Phys.*, **48**, 129.

[11] Madden, P. A., and Tildesley, D. J., 1983, *Molec. Phys.*, **49**, 193.

[12] Steele, W. A., 1985, *Molec. Phys.*, **56**, 415.

[13] Dorfmüller, Th., and Samios, J., 1984, *Molec. Phys.*, **53**, 1167.

[14] Samios, J., Mittag, U., and Dorfmüller, Th., 1985, *Molec. Phys.*, **56**, 541.

[15] Berns, R. M., Wormer, P. E. S., Mulder, F., and van der Avoird, A., 1978, *J. chem. Phys.*, **69**, 2102. Wormer, P. E. S., and van Dijk, G., 1979, *J. chem. Phys.*, **70**, 5695. Schäfer, J., and Meyer, W., 1984, *Electronic and Atomic Collisions*, edited by J. Eichler, I. V. Hertel and N. Stolterfoht (Elsevier Science Publishers), p. 529.

[16] BUCKINGHAM, A. D., 1967, *Adv. chem. Phys.*, **12,** 107.
[17] BIRNBAUM, G., 1978, *Intermolecular Spectroscopy and Dynamical Properties of Dense Systems,* International School of Physics 'Enrico Fermi', Varenna, 24 July–5 August; see also POLL, J. D., and HUNT, J. L., 1981, *Can. J. Phys.*, **59,** 1148. BIRNBAUM, G., and SUTTER, H., 1981, *Molec. Phys.*, **42,** 21.
[18] VERLET, L., 1976, *Phys. Rev.*, **98,** 159. SINGER, K., TAYLOR, A., and SINGER, J. V. L., 1977, *Molec. Phys.*, **33,** 1757.
[19] EVANS, D. J., 1977, *Molec. Phys.*, **34,** 317. FINCHMAN, D., *Information Quarterly—CCPS,* No. 2, September 1981, p. 6.
[20] BOGARD, M. P., BUCKINGHAM, A. D., PIERENS, R. K., and WHITE, A. H., 1978, *Trans. Faraday I,* **74,** 3008.
[21] BATTAGLIA, M. R., BUCKINGHAM, A. D., NEUMARK, D., PIERENS, R. K., and WILLIAMS, J. H., 1981, *Molec. Phys.*, **43,** 1015.
[22] AMOS, R. D., and BATTAGLIA, M. R., 1978, *Molec. Phys.*, **36,** 1517.
[23] GIBSON, I. P., and DARE, J. C., 1981, *Molec. Phys.*, **42,** 83.